Investigating extreme ultraviolet radiation chemistry with first-principles quantum chemistry calculations

Jonathan H. Ma,[a,b] Han Wang,[c] David Prendergast,[c] Andrew Neureuther,[a,d] and Patrick Naulleau[a,*]

[a]Lawrence Berkeley Laboratory, Materials Sciences Division, Center of X-Ray Optics, Berkeley, California, United States

[b]University of California Berkeley, Department of Physics, Berkeley, California, United States

[c]Lawrence Berkeley Laboratory, Molecular Foundry, Berkeley, California, United States

[d]University of California Berkeley, Department of Electrical Engineering and Computer Science, Berkeley, California, United States

Abstract. In extreme ultraviolet (EUV) lithography, chemistry is driven by secondary electrons. A deeper understanding of these processes is needed. However, electron-driven processes are inherently difficult to experimentally characterize for EUV materials, impeding targeted material engineering. A computational framework is needed to provide information for rational material engineering and identification at a molecular level. We demonstrate that density functional theory calculations can fulfill this purpose. We first demonstrate that primary electron energy spectrum can be predicted accurately. Second, the dynamics of a photoacid generator upon excitation or electron attachment are studied with *ab-initio* molecular dynamics calculations. Third, we demonstrate that electron attachment affinity is a good predictor of reduction potential and dose to clear. The correlation between such calculations and experiments suggests that these methods can be applied to computationally screen and design molecular components of EUV material and speed up the development process. © *2020 Society of Photo-Optical Instrumentation Engineers (SPIE)* [DOI: 10.1117/1.JMM.19.3.034601]

Keywords: extreme ultraviolet lithography; extreme ultraviolet exposure chemistry; photoacid generator chemistry; radiation chemistry; extreme ultraviolet fundamentals.

Paper 20016 received Apr. 15, 2020; accepted for publication Aug. 4, 2020; published online Aug. 27, 2020.

1 Introduction

With the introduction of extreme ultraviolet (EUV), electron-driven processes in photoresists become relevant. In deep ultraviolet (DUV), resists operate with photochemistry.[1] Photochemistry is specific and relatively well studied,[1,2] making function-specific engineering possible. For example, it is understood that photon absorption is only useful if it happens at the photoacid generator (PAG). As a result, polymers are engineered to be transparent and the UV absorption cross-sections are to be optimized to maximize quantum efficiency. In EUV, upon photon absorption, a high kinetic energy primary electron is very likely to be produced as a result. Such primary electrons are very unlikely to initiate chemistry immediately; instead, they rapidly lose energy through generating a cascade of low kinetic energy secondary electrons.[3] In the context of chemically amplified resists (CARs), the PAG can be activated through internal excitation[4] or low kinetic energy electron attachment,[3] which is hypothesized to be the main driver of EUV chemistry. From photon absorption to PAG activation, there are now extra steps involving electrons. As electron interaction with matter is nondiscriminative, electrons interact with any species. As a result, all constituents of the photoresist participate in the photon-to-chemistry conversion. Understanding these electron processes is vital for several reasons. Since more than one secondary electron is generated, the quantum efficiency (absorbed photon-to-acid conversion ratio) of EUV resists can be larger than unity and is currently known

*Address all correspondence to Patrick Naulleau, E-mail: pnaulleau@lbl.gov

to be around 2 to 3.[5,6] Leveraging our knowledge in EUV radiation chemistry processes allows us to further improve the quantum yield, which comes with the obvious benefit of reducing dose to clear. On top of that, optimizing the quantum yield is shown to bring us closer to the photon shot noise limit of stochastics.[7] Lastly, the extra efficiency provided by increased quantum efficiency enables more flexible use of contrast enhancing mechanisms such as photodecomposable quencher.[8]

Individual electron processes in condensed phase are difficult to characterize. Therefore, first-principle quantum chemistry calculations can provide insights to such processes or even predict yield. To accurately describe the chemistry of a material, an accurate description of the electronic structure is needed, leaving us with density functional theory (DFT)[9] or wave function methods such as coupled-cluster singles and doubles (CCSD).[10] DFT-based first-principle calculations have a few advantages. Compared to wave function-based methods such as CCSD, it has a better resource scaling (N^3 to N^4 of DFT/hybrid-DFT versus N^5 to N^6 of CCSD[11]), thus making it a more viable method for studying large molecules and systems.

In this article, we demonstrate four types of DFT-based calculations. First, the primary electron energy distribution could affect the electron blur and the generation efficiency of secondary electrons. We present our ionization calculations, which predict primary electron energy spectra. For a PAG to be efficient, it should be able to break apart readily if it is internally excited or has captured an extra electron. To characterize the likelihood of the PAG breaking apart, *ab-initio* molecular dynamics (AIMD) calculations, which track the forces acting on each individual atom at room temperature, were carried out to study and compare the two activation mechanisms. The dynamics calculations address the questions regarding the outcome, provided an extra electron is attached. The yield, however, also depends on how likely an electron attaches to the PAG. To that end, we report that electron attachment calculations can be applied to predict reduction potential and dose to clear.

2 Ionization Calculations

Upon absorption of an EUV photon, photoionization occurs, resulting in a primary electron.[12] The kinetic energy carried by these electrons might have implications on the resolution and dose of a resist. Intuitively, with a higher kinetic energy, an electron takes more space to deposit energy but generates fewer secondary electrons. Currently, the electron blur has been estimated to be in the order of a few nanometers[5,6] while the kinetic energy of primary electrons in typical polymer material has been identified to be between 80 and 85 eV.[13] At the current node, in CARs, electron blur is still small compared with acid blur. However, in other platforms, effective electron blur might be a major contributor to resolution.

The kinetic energy of a primary electron is the excitation energy (92 eV) minus the binding energy of the electron. Before ionization, electrons reside in molecular orbitals. The binding energy of an electron is calculated by taking the total energy difference in the molecule between the ground state and the excited hole state resulted from ionization. By calculating such an energy difference for electrons from different orbitals, the binding energy spectrum, thus primary electron kinetic energy spectrum, can be calculated. Ionization calculations are implemented with the package Q-Chem 5.1.2[14] running on Scientific Linux 7 based computing cluster. The total energies are obtained using DFT. The PBE0 hybrid functional and the Ahlrich's triple-zeta basis set with polarization and diffuse functions (def2-TZVPD) are used. The excited hole energy was calculated with the maximum overlap method.[15,16] All computations are carried out at the Nano cluster at Lawrence Berkeley Laboratory's Laboratory Research Computing facility (LBL-LRC) using a single node (each with two 4-core Xeon X5550 processors and 24 GB of memory).

For polymer-based resists, engineering of low kinetic energy primary electrons has been investigated by incorporating halogens. Kostko et al.[17] demonstrated that, by incorporating bromine or iodine into prototypical monomers, low kinetic primary electrons are measured in gas-phase photoemission experiments. On top of that, a series of halogenated polymers were investigated, and their primary electron energy spectra were measured with gas-phase photoemission. We perform ionization calculation on these halogenated methylphenols. In Fig. 1,

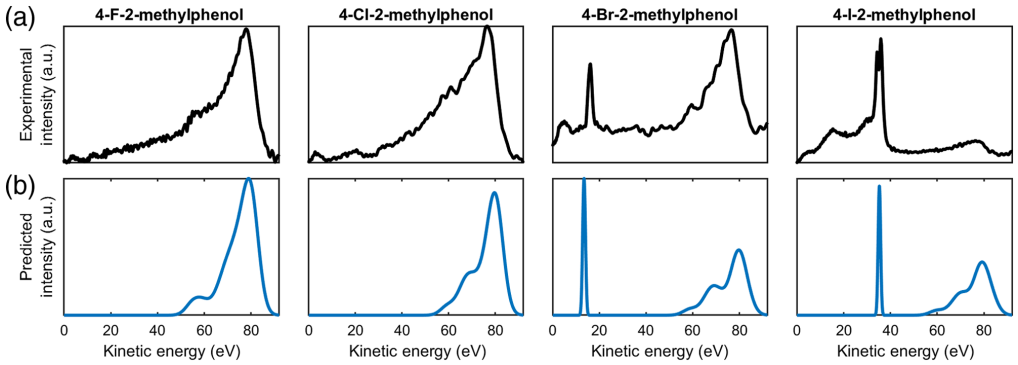

Fig. 1 (a) Experimental primary electron energy spectrum from Ref. 18. (b) Theoretical prediction from binding energy calculations. Low kinetic energy (<40 eV) features are broadened by 0.5 eV and high kinetic energy features (>40 eV) are broadened by 3 eV.

the experimental spectra measured in Ref. 17 are adapted and presented in the upper row. In the lower row, our theoretical predictions are presented. The binding energies of orbitals are discrete. In reality, there are thermal broadening and finite instrumental resolution. The finite lifetime of the excited hole also leads to broadening. The discrete peaks are therefore broadened to account for these effects. Electrons with high kinetic energy (>40 eV) are shallowly bounded (low binding energy), and they are sensitive to temperature effects. A broadening of 3 eV is applied to them. Electrons with kinetic energy lower than 40 are semicore in nature and are not very susceptible to thermal effects so they are only broadened by 0.5 eV to emulate the finite resolution of the detector and the finite lifetime of the excited hole.

As can be seen in Fig. 1, the energy positions of the features line up reasonably well between theoretical and experimental spectra. The feature near 85 eV is captured by all calculations. The low kinetic energy generated by brominated and iodinated monomers is also well predicted by our calculations.

The only input needed for these calculations is molecular structures. The agreement between experiments and theoretical calculations indicates that density functional-based ionization calculation is a useful tool for predicting the energy of primary electrons.

However, we note that there are features that the ionization calculations cannot explain. First of all, in iodinated monomers, experimentally, the intensity of the low kinetic energy feature is much stronger than their high kinetic energy counterpart. This is not captured in the calculation because the matrix element is not calculated. Our current framework for ionization only provides information as to where the electrons are in terms of energy. To accurately reproduce the spectrum, the probability that an electron is ejected from a given orbital is also needed. Such probability is different for different orbitals and can be predicted with matrix element calculation.[18] The current implementation of Q-Chem presents difficulties for such calculations at EUV excitation energy. However, custom implementation of matrix element calculations with EUV excitations can be explored in open-source packages.

The other unexplained feature in the iodinated monomer is the broad features at low kinetic energies. Those electrons have been demonstrated to be Auger electrons.[17] Auger electron spectrum can be predicted with many-body wave function methods.

By combining ionization Auger electron calculations, the primary electron energy spectrum can be predicted accurately. Such spectra can be used to generate realistic primary electron energy distribution in Monte Carlo trajectory simulations.

3 Internal Excitation

Internal excitation as a PAG activation mechanism has been shown to be present in EUV resists.[4] As Narasimhan et al.[4] suggested, however, the quantum efficiency is only on the order of 0.1. Understanding internal excitation at a fundamental level could allow us to identify strategies to improve the quantum efficiency of this process in EUV materials.

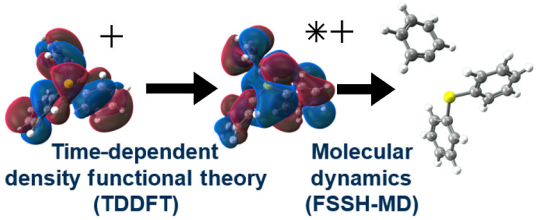

Fig. 2 Schematic for the computational method used for internal excitation.

Internal excitation is a process through which a molecule (in the context of CARs, a PAG) is promoted to an excited state by an electron that propagates nearby. The propagating electron generates a time-varying electric field as observed by a stationary PAG. The PAG is essentially subjected to broadband electromagnetic radiation. If the spectrum of the radiation overlaps with the absorption spectrum of the PAG, the PAG can be excited optically (Fig. 2). The PAG is not ionized nor is the electron captured by the PAG in the process. In an excited state, the PAG molecule becomes unstable and becomes susceptible to breaking apart. To study this effect, time-dependent DFT calculations are used. The forces acting on each atom in a molecule can be evaluated for each excited state, thus the motion of the molecule can be calculated. Such calculations are implemented with the AIMD module of Q-Chem. In an excited state, a molecule has a finite chance of transitioning into another excited state.[19] To account for such transitions, fewest switches surface hopping (FSSH) coupling is included in the dynamics calculations. All calculations are carried out using a single-node Vulcan cluster (each with two 4-core XEON E5530 processors and 24 GB of memory) at LBL-LRC.

We hope to achieve two goals with our excited state dynamics calculations. First, to reproduce certain known chemistry to validate our dynamics calculations. Second, because measurements of yield are seldom direct,[3,20] such calculations can provide a clean way of characterizing the propensity of a PAG to break apart upon excitation.

Triphenyl sulfonium (TPS) triflate (-OTf) is well studied and has very well-understood chemistry at DUV.[2,20,21] Upon optical excitation, cleavage of a sulfur-carbon (S─C) bond was demonstrated to be the immediate outcome.[3,22] As demonstrated in Ref. 4, internal excitation is very similar to optical excitation. We, therefore, anticipate that S─C bond cleavage as a direct result of internal excitation as well.

AIMD-FSSH calculations with excited states are extremely expensive. With the presence of light atoms such as hydrogen, the largest achievable time step was 241 attosecond, requiring around 1000 steps to study bond-breaking processes that typically take hundreds of femtoseconds.[23] To keep computation time reasonable, the anion is ignored as chemistry is driven by the TPS cation. On top of that, we use a smaller basis set—the double zeta cc-pVDZ basis set in conjunction with the functional PBE0. Mechanical properties, such as geometry, were demonstrated to be less sensitive to basis size.[24] Moreover, with the absence of the anion, the subject is a cation with tightly bound orbitals, rendering diffuse functions unnecessary.

At room temperature, the molecule is subjected to thermal perturbations. That has to be factored into the initial geometry and velocity of the simulation. Also, as the reaction continues, such perturbation has to be included in the evolution of the molecule. To acquire an ensemble of realistic initial conditions, the molecule is first allowed to evolve at room temperature. About 50 geometries/velocity were then taken from that evolution and used as initial conditions for the dynamics calculation. We promote the molecule to its first and 11^{th} excited states to understand its evolution upon excitation. And in all cases, the TPS PAG is simulated for 241 fs.

Our simulations indicate that there are two possible outcomes, either the TPS PAG remains intact or a S─C bond is cleaved and a phenyl ring is ejected. With this knowledge, we can characterize the reaction with the S─C (of the phenyl ring that ends up the furthest away from the sulfur) bond length.

The bond length is around 1.7 to 1.8 Å in all initial configurations and its distribution is represented with blue bars in Fig. 3. We use 2 Å as a cutoff for bond cleavage. After the evolution, the distribution of S─C bond length is shown with orange bars. In 49 out of 50 initial conditions, cleavage occurs if the PAG is promoted to its first excited state. By promoting the

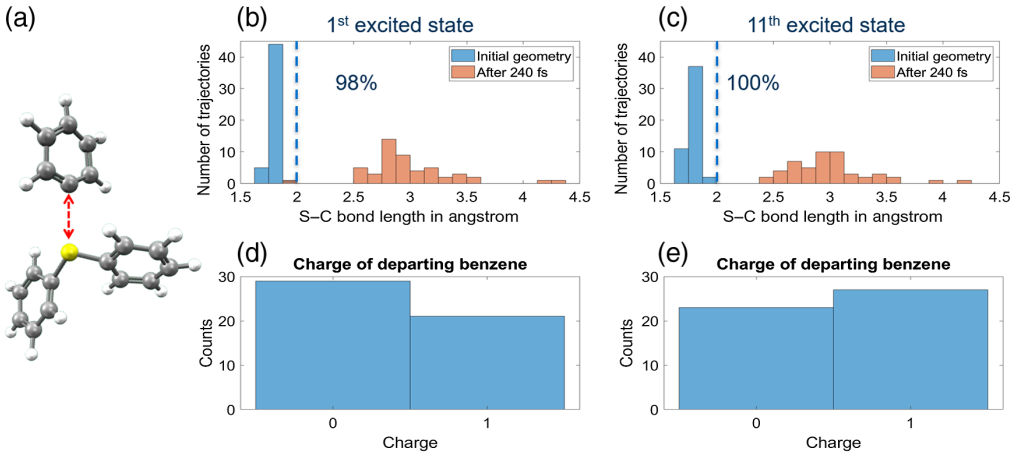

Fig. 3 Results for internal excitation AIMD calculations. The cleavage of C–S bond is shown in (a) with the red dashed arrow indicating the bond length. The distributions of bond lengths before and after evolutions initiated in the first and the 11th excited states are shown in (b) and (c). The charge carried by the departing benzene in the two initial conditions is shown in (d) and (e).

PAG into its 11th excited state, the outcome is qualitatively the same—S–C bond cleavage is found to be the only chemical outcome and the yield is nominally 100%.

The charge carried by the ejected phenyl ring was also calculated using the Mulliken population analysis.[25] By exciting a TPS PAG to a higher excited state, the benzene ring is more likely to be positively charged. While this is consistent with previous experimental work,[20] the difference is too small to be conclusive with 50 trajectories.

4 Postattachment Dynamics

The main driver of EUV chemistry is low kinetic energy electron attachment.[26] The efficiency of this process depends on the likelihood of the PAG to break apart after electron attachment. AIMD calculations can be used to understand the dynamics of the PAG subsequent to electron attachment as well.

As in internal excitation, 50 realistic initial geometries and velocities were prepared for the TPS cation. For each of these conditions, an extra electron is added. Assuming the incident electron is almost thermalized, the molecule is assumed to be in ground state. With ground state as a starting point, FSSH coupling is not needed. AIMD calculations are again made with PBE0 functional and the double zeta cc-pVDZ basis.

Similar to internal excitation, there are only two possible outcomes—the PAG either remains intact or ejects a phenyl ring by S–C cleavage. The outcome is characterized similarly. Figure 4 shows the initial and final distributions of carbon-sulfur (C–S) bond length. After 240 fs of evolution, with a 2-Å cutoff, a S–C bond breaks in 47 out of the 50 initial conditions, indicating that the yield is around 94%. Compared to internal excitation, the distribution of final C–S bond length in postattachment dissociation is broader yet the expectation value of the bond length is

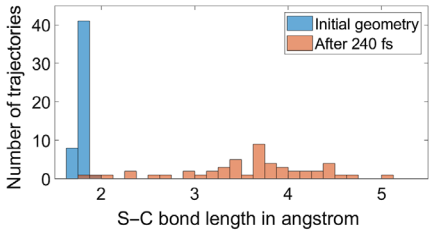

Fig. 4 The distributions of bond lengths before and after evolutions initiated with electron attachment at ground state.

larger. The charge carried by the ejected phenyl ring is found to be zero in all initial conditions. Although this result suggests that electron attachment does not lead to heterolysis, we would like to point out that the simulations take place in vacuum. Real resists are likely dielectric media. Therefore, a logical extension of this study will be incorporating dielectric medium into molecular dynamics calculations.

5 Reactions after S–C Bond Cleavage

In the broader context of TPS PAG chemistry, the cleavage of S–C bond, the subject of the study, is merely the beginning of a series of chemical reactions. Due to the volatile nature of the immediate products of S–C bond cleavage, they react readily. The in-cage or cage escaped products previously reported[2,22] are understood to be results of the fragments reacting with each other or the substrate, suggesting that S–C bond cleavage initiates the entire process.[2,20,22] This work demonstrates that the cleavage of the S–C bond can be predicted with AIMD calculations. However, the formation of products further downstream, such as in-cage produces where the phenyl fragments recombine, involves environment-dependent reactions. For example, the lifetime of the ejected phenyl depends on the density and moiety of the surrounding. To accurately predict the outcome of these reactions, an accurate description of the environment is needed. Therefore, the size of the system would have to be increased dramatically. Further investigations into methods specialized for large systems are required for scalable investigations of the interaction of the active species in their surroundings.

6 Electron Attachment

Electron affinity and its effect on PAG performance have been studied[27] showing that, if a PAG can be reduced more easily in a cyclic voltammetry, resists consisting of that PAG have a lower dose to clear.[28]

To estimate the electron affinity computationally, we compute the lowest unoccupied molecular orbital (LUMO) energy of the four onium PAGs used in Ref. 28 and use it as a proxy for electron attachment affinity. In Ref. 28, the reduction potential is measured with the PAGs dissolved in acetonitrile while in condensed phase, the PAGs are tightly bound to their nonaflate counter anion.

Vertical electron affinity computations are inherently unstable for neutral species due to the presence of orthogonal discretized continuum (ODC) states.[25] Since onium PAGs in polymer resists are tightly bound to their counter anion, a method suitable for neutral species should be used. The aforementioned issues with ODC states can be systematically mitigated but doing so is computationally costly. Instead, we seek to empirically identify the most predictive functional/basis combinations that are the least susceptible to ODC states.

The predictive power of our method is studied empirically, as shown in Figs. 5 and 6. The first vertical electron affinities of 30 hydrocarbons[24] and four deoxyribose nucleic acid nucleobases[29] have been reported. A total of 34 molecules are included. Their molecular geometries are optimized with the PBE0 functional and def2-SVPD basis. The LUMO energies of the molecules are then calculated using various combinations of functionals and basis sets. Two metrics are used to assess the predictive power. First, correlation between experimental values and the LUMO energies is compared for each combination is used. Second, the root-mean-square error (RMSE) is reported for each method. The same procedure is repeated with the DNA nucleobases removed (Fig. 5) to understand the robustness of the methods.

The functionals PBE, PBE0, B3LYP, B2PLYP, PBE-QIDH, and ωB97X-D were tested. PBE0, B3LYP, and ωB97X-D are found to be the best compromise. Three functionals are selected altogether to ensure there is a qualitative agreement between them. As shown in Fig. 6 and Table 1, the improvements in statistical correlation from PBE to PBE0 indicate that inclusion of exact exchange[30] improves prediction. Double hybrids (B2PLYP/PBE-QIDH) incorporate MP2 electronic dynamic correlation, which does not improve performance significantly. Yet the computational time scaling is increased by an order of magnitude (from $N_{basis}{}^4$ of

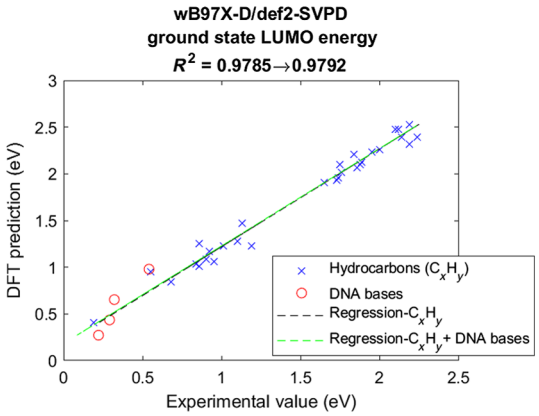

Fig. 5 Example of assessment of predictive power of a single functional/basis combination. Each of the blue crosses and red circles represents a molecule. Linear regression is performed with (green dotted line) and without (black dotted line) DNA bases to infer the robust of the combination. R^2, which is identical to correlation coefficient squared in linear regression, is 0.9785 (hydrocarbons only) and 0.9792 (hydrocarbons and DNA bases).

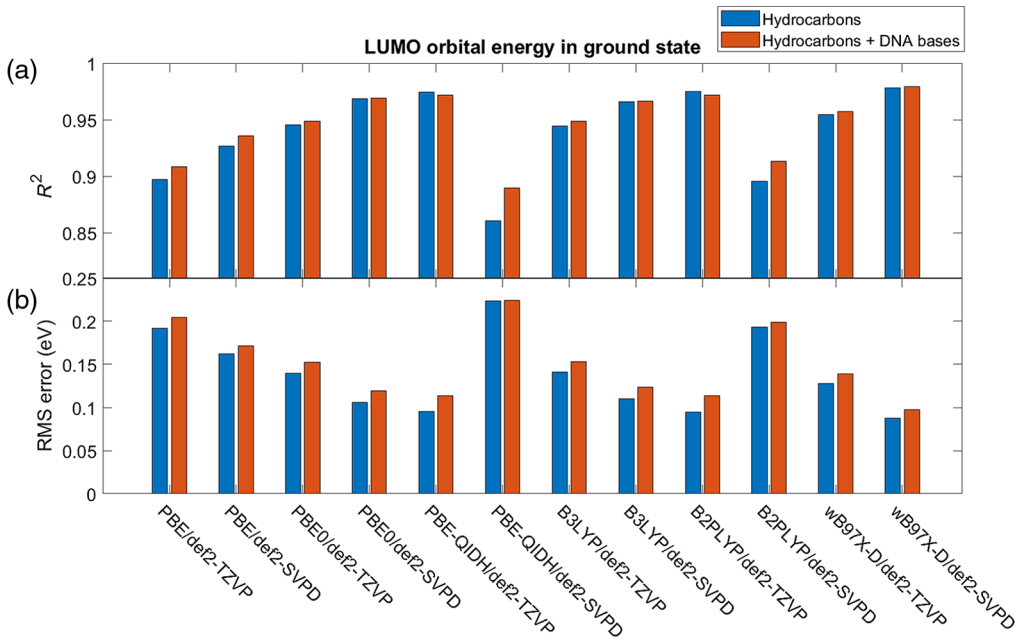

Fig. 6 Predictive powers of different functional/basis combinations. Coefficient of correlation between experimental data and predictions is shown in (a). RMSE (regression slope) is shown in (b). Two colors represent two different datasets used for regression.

B3LYP/PBE0 to N_{basis}^5 of B2PLYP/PBE-QIDH).[11] Moreover, as shown in Fig. 6 and Table 1, double hybrid functionals are very basis sensitive in terms of their performance.

All electron affinity calculations are carried out at the Nano or Etna cluster at LBL-LRC using the package Q-Chem 5.1.2. A single Etna node (with 2 12-core Xeon E5-2670 v3 processors and 64 GB of memory) or three Nano nodes (each with 2 4-core Xeon X5550 processors and 24 GB of memory) were used for functional assessment. For PAG molecules, given their sizes, either two Etna nodes or four Vulcan nodes (each with 2 4-core XEON E5530 processors and 24 GB of memory) are used.

For the three selected functionals, it is consistent that def2-SVPD is more robust than def2-TZVP. The latter is supposedly a bigger basis set that provides better descriptions of molecules. The superiority of the former indicates the importance of diffuse functions in such calculations.

Table 1 Parameters for linear model between experiments and DFT for various functionals. The linear model is $E_{\text{experiment}} = mE_{\text{DFT}} + C$. The coefficients of correlation and RMSE are also included.

Functional/basis	Slope (m)	Intercept (C)	R^2	RMSE (eV)
wB97X-D/def2-SVPD	0.9589	−0.1774	0.9792	0.0975
B2PLYP/def2-TZVP	0.9944	0.0990	0.9718	0.1137
PBE-QIDH/def2-TZVP	0.9504	−0.4156	0.9717	0.1139
PBE0/def2-SVPD	0.9803	1.5328	0.9689	0.1192
B3LYP/def2-SVPD	1.0187	1.7800	0.9665	0.1239
wB97X-D/def2-TZVP	0.9268	−0.1837	0.9576	0.1393
PBE0/def2-TZVP	0.9703	1.4788	0.9490	0.1528
B3LYP/def2-TZVP	0.9967	1.7139	0.9488	0.1531
PBE/def2-SVPD	1.0162	2.5272	0.9360	0.1711
B2PLYP/def2-SVPD	1.1811	0.0900	0.9136	0.1989
PBE/def2-TZVP	1.0022	2.4603	0.9084	0.2048
PBE-QIDH/def2-SVPD	1.1865	−0.5701	0.8898	0.2245

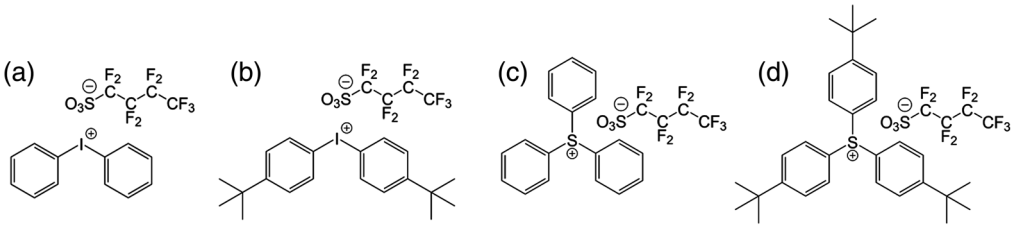

Fig. 7 The four onium PAGs investigated. (a) Diphenyliodonium nonaflate, (b) bis (4-tert-butylphenyl)iodonium (BTBPI) nonaflate, (c) TPS nonaflate, and (d) tris(4-tert-butylphenyl)sulfonium nonaflate.

In Ref. 28, the reduction potential and dose to clear of four onium PAGs (Fig. 7) were reported. In the reduction potential measurement, the PAG is dissolved in acetonitrile, resulting in ionic dissociation. In actual resist, the PAG is likely to be bound to its counter anion. The two cases need to be treated separately.

To make accurate predictions about onium PAGs in acetonitrile, two factors have to be accounted for. First, as a result of ionic dissociation, the counter anion is no longer in the vicinity of chemically active onium ion. Second, the presence of acetonitrile has to the accounted for. The vertical electron affinity of the onium ions is calculated in conjunction with polarizable continuum model (pcm), which captures the physics of polar solvents[31] and is implemented in the Q-Chem package.

In all three hybrid functionals, the experimental reduction potential and the computation vertical electron affinities, calculated from the molecular LUMO energies, form a linear relationship (Fig. 8). Additionally, all three functionals give qualitatively similar results, meaning that the correlation between the two is not theory dependent and thus we expect the calculations to be robust. As the data points lie close to the line of the best linear fit, the regression line can be used to predict the experimental reduction potential from computational vertical attachment energies with reasonable confidence.

We move on to calculate the vertical electron affinities of the onium triflates in the presence of the counter anion, which is representative of their behavior in condensed phase. As shown in

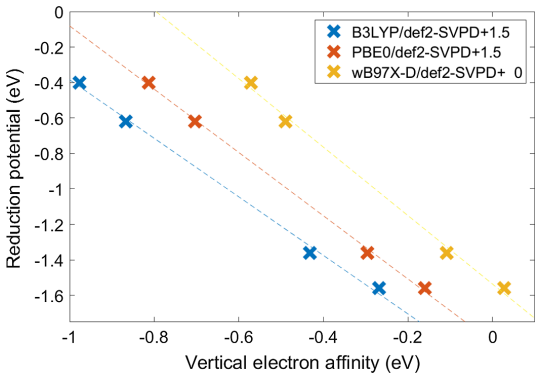

Fig. 8 Computational vertical electron affinity of four onium PAG cations calculated in conjunction with pcm versus experimentally measured reduction potential reported in Ref. 29. Dashed lines are linear fits.

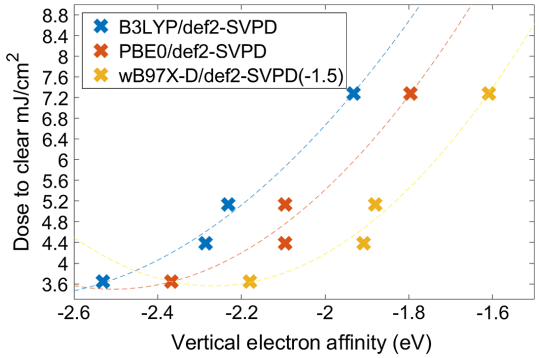

Fig. 9 Computational vertical electron affinities of four onium PAGs versus dose to clear reported in Ref. 29. Dashed lines are quadratic fits.

Fig. 9, the vertical attachment energies correlate well with the experimental dose to clear. In this case, however, a quadratic function is a better fit.

It has been reported that using another computational approach, the AM-1 semiempirical method, the correlation between vertical electron affinity and dose to clear was not identified.[27] In Ref. 27, the effect of electron affinity was studied with a different series of molecules. The most notable difference is that the engineered electron grabbing species are heterocyclic—they have two of the three phenyl rings connected. As the efficiency of dissociative electron attachment depends on both the attachment of the electron and the likelihood of dissociation, having the immobilized aryl groups could impede dissociation, offsetting the benefits of lower vertical electron affinity.

Subsequent molecular dynamics study is being explored to investigate the effect of heterocyclic aryl groups in TPS, such as onium PAGs, to understand the trade-off between attachment affinity and dissociation impedance.

7 Conclusion

In summary, four electron processes in EUV exposure radiation chemistry were studied by density functional-based calculations. First, it was demonstrated that primary electron energies of prototypical monomers can be accurately predicted with ionization calculations. Second, AIMD calculations were shown to reproduce the immediate outcome of internal excitation. Moreover, the yield of bond cleavage could be predicted with such calculations. Third, molecular dynamics calculations can also be used to predict the outcome of low kinetic energy electron attachment. It was shown that, upon electron attachment, the chemical outcome is similar to internal excitation

and the bond cleavage probability is around 90% to 95%. Finally, vertical electron affinity taken from calculations made with proper assumptions about the environment predicts reduction potential well. With the series of onium PAG with unconnected ligands, the dose to clear correlates with the vertical electron affinity of the PAG very well.

In the context of CARs, a combination of such calculations can be used to further understand PAG processes and ultimately improve their performance. The processes studied also take place in other resist platforms, and the relevant calculations can be adapted to other systems with minimal effort.

Acknowledgments

We acknowledge Oleg Kostko for his advice on spectroscopy and Daniel Slaughter for his advice on electron chemistry. H.W. and D.P. are supported by the Molecular Foundry at Lawrence Berkeley National Laboratory. Computation resources are provided by the theory facility at the Molecular Foundry as part of an internal research project. J.H.M. is sponsored by Center for Design-Enable Nanofabrication (C-DEN). Member companies include ASML, Carl Zeiss Group, Intel, KLA-Tencor, Mentor Graphics, and Samsung. This work was performed in part at Lawrence Berkeley National Laboratory, which is operated under the auspices of the Director, Office of Science, of the U.S. Department of Energy under Contract No. DE-AC02-05CH11231. This work was originally submitted as a conference proceeding for the International Conference on Extreme Ultraviolet Lithography (2019) (https://doi.org/10.1117/12.2538558)

References

1. W. D. Hinsberg and G. M. Wallraff, "Lithographic resists," in *Encyclopedia of Polymer Science and Technology*, H. F. Mark, Ed., John Wiley and Sons, San Francisco, California (2012).
2. S. Tagawa et al., "Radiation and photochemistry of onium salt acid generators in chemically amplified resists," *Proc. SPIE* **3999**, 204–213 (2000).
3. T. Kozawa and S. Tagawa, "Radiation chemistry in chemically amplified resists," *Jpn. J. Appl. Phys.* **49**, 030001 (2010).
4. A. Narasimhan et al., "Studying electron-PAG interactions using electron-induced fluorescence," *Proc. SPIE* **9779**, 97790F (2016).
5. S. Grzeskowiak, R. L. Brainard, and G. H. Denbeaux, "Measuring extreme-ultraviolet secondary electron blur (Conference Presentation)," *Proc. SPIE* **10960**, 1096007 (2019).
6. T. Kozawa and S. Tagawa, "Thermalization distance of electrons generated in poly(4-hydroxystyrene) film containing acid generator upon exposure to extreme ultraviolet radiation," *Jpn. J. Appl. Phys.* **50**, 030209 (2011).
7. P. Naulleau and G. Gallatin, "Relative importance of various stochastic terms and EUV patterning," *J. Micro/Nanolithogr. MEMS MOEMS* **17**, 041015 (2018).
8. L. Long, A. R. Neureuther, and P. P. Naulleau, "Modeling of novel resist technologies," *Proc. SPIE* **10960**, 1096011 (2019).
9. W. Kohn and L. J. Sham, "Self-consistent equations including exchange and correlation effects," *Phys. Rev.* **140**, A1133–A1138 (1965).
10. O. Sinanoğlu, "Many-electron theory of atoms and molecules. I. Shells, electron pairs vs many-electron correlations," *J. Chem. Phys.* **36**, 706–717 (1962).
11. F. Jensen, *Introduction to Computational Chemistry*, Wiley, Hoboken, New Jersey (2017).
12. D. F. Ogletree, "Molecular excitation and relaxation of extreme ultraviolet lithography photoresists," Chapter 2 in *Materials and Processes for Next Generation Lithography*, Vol. 11, A. Robinson and R. Lawson, Eds., pp. 91–113, Elsevier, Amsterdam, Netherlands (2016).
13. J. Ma, A. R. Neureuther, and P. P. Naulleau, "Investigating EUV radiochemistry with condensed phase photoemission," *Proc. SPIE* **10957**, 109571Y (2019).
14. Y. Shao et al., "Advances in molecular quantum chemistry contained in the Q-Chem 4 program package," *Mol. Phys.* **113**, 184–215 (2015).

15. N. A. Besley, A. T. B. Gilbert, and P. M. W. Gill, "Self-consistent-field calculations of core excited states," *J. Chem. Phys.* **130**, 124308 (2009).
16. A. T. B. Gilbert, N. A. Besley, and P. M. W. Gill, "Self-consistent field calculations of excited states using the maximum overlap method (MOM)," *J. Phys. Chem. A* **112**, 13164–13171 (2008).
17. O. Kostko et al., "Fundamental understanding of chemical processes in extreme ultraviolet resist materials," *J. Chem. Phys.* **149**, 154305 (2018).
18. J. J. Yeh and I. Lindau, "Atomic subshell photoionization cross sections and asymmetry parameters: $1 \leqslant Z \leqslant 103$," *At. Data Nucl. Data Tables* **32**, 1–155 (1985).
19. J. C. Tully, "Molecular dynamics with electronic transitions," *J. Chem. Phys.* **93**, 1061–1071 (1990).
20. E. Despagnet-Ayoub et al., "Triphenylsulfonium topophotochemistry," *Photochem. Photobiol. Sci.* **17**(1), 27–34 (2018).
21. Y. Matsui et al., "Difference in reaction schemes in photolysis of triphenylsulfonium salts between 248 nm and dry/wet 193 nm resists," *Appl. Phys Express* **1**, 036001 (2008).
22. J. L. Dektar and N. P. Hacker, "Photochemistry of triarylsulfonium salts," *J. Am. Chem. Soc.* **112**, 6004–6015 (1990).
23. K. D. Closser et al., "The importance of inner-shell electronic structure for enhancing the EUV absorption of photoresist materials," *J. Chem. Phys.* **146**, 164106 (2017).
24. S. W. Staley and J. T. Strnad, "Calculation of the energies of. pi.* negative ion resonance states by the use of Koopmans' theorem," *J. Phys. Chem.* **98**, 116–121 (1994).
25. R. S. Mulliken, "Electronic population analysis on LCAO–MO molecular wave functions. I," *J. Chem. Phys.* **23**, 1833–1840 (1955).
26. T. Kozawa et al., "Analysis of acid yield generated in chemically amplified electron beam resist," *J. Vac. Sci. Technol. B* **24**, 3055–3060 (2006).
27. D. L. Goldfarb, A. Afzali-Ardakani, and M. Glodde, "Acid generation efficiency: EUV photons versus photoelectrons," *Proc. SPIE* **9779**, 97790A (2016).
28. S. Grzeskowiak et al., "Electron trapping: a mechanism for acid production in extreme ultraviolet photoresists," *J. Micro/Nanolithogr. MEMS MOEMS* **17**, 033501 (2018).
29. K. Aflatooni, G. A. Gallup, and P. D. Burrow, "Electron attachment energies of the DNA bases," *J. Phys. Chem. A* **102**, 6205–6207 (1998).
30. J. P. Perdew, M. Ernzerhof, and K. Burke, "Rationale for mixing exact exchange with density functional approximations," *J. Chem. Phys.* **105**, 9982–9985 (1996).
31. V. Barone and M. Cossi, "Quantum calculation of molecular energies and energy gradients in solution by a conductor solvent model," *J. Phys. Chem. A* **102**, 1995–2001 (1998).

Biographies of the authors are not available.